Zeitschrift für anorganische und allgemeine Chemie

WILEY VCH

Journal of Inorganic and General ZAAC Zeitschrift für anorganische und allgemeine Chemie

RESEARCH ARTICLE OPEN ACCESS

A New Thallide Auride Double Salt: $Cs_{3.4}K_{4.6}[Au][Tl_7]$ Featuring $[Tl_7]^{7-}$ Zintl Clusters

Vanessa F. Schwinghammer[1,2] | Stefanie Gärtner[1,2]

[1]Department of Inorganic Chemistry, University of Regensburg, Regensburg, Germany | [2]Central Analytics, University of Regensburg, Regensburg, Germany

Correspondence: Stefanie Gärtner (Stefanie.Gaertner@ur.de)

Received: 27 August 2025 | **Revised:** 3 November 2025 | **Accepted:** 3 November 2025

Keywords: alkali metal | auride | DFT | thallium | X-ray

ABSTRACT

$Cs_{3.4}K_{4.6}[Au][Tl_7]$ has been prepared from the elements (*Pnma*, $a = 39.6898(12)$ Å, $b = 12.0407(4)$ Å, $c = 10.9334(3)$ Å, $V = 5225.0(3)$ Å^3, $Z = 8$, $R_1/wR_2 = 0.0556/0.0935$). Band structure calculations reveal a small bandgap at E_F (0.10139 eV).

1 | Introduction

The majority of the elements are categorized as metals. In this context, it is not surprising that a combination of two or more metals results in a great variety of materials. Most of those intermetallic compounds and phases can be described as solid solutions, Frank Kasper, Laves, Hume–Rothery, or Zintl phases [1]. The last type was first introduced by Eduard Zintl himself in the 1930s [2, 3]. The resulting concept, which Klemm and Busmann later modified, describes a formal electron transfer from the less electronegative to the more electronegative element under the formation of (poly)anions [4]. The first and still classical example of a Zintl phase is NaTl, although it lies left of the so-called Zintl border [2, 5, 6].

The field of alkali metal thallides again attracted attention between the early 1990s and the 2010s [7, 8]. In general, the respective compounds can be described as materials at the frontier between a salt-like and metallic nature, which depends on the valence electron concentration [8, 9]. While up to a composition of $A_{15}Tl_{27}$ (A = K-Cs) [10, 11], two- or three-dimensional thallium networks are formed, isolated clusters can be found at higher atomic alkali metal proportions [8]. Most of the compounds have been described as electron precise with one to four different cluster types. Examples for exceptions are A_8Tl_{11} (A = K-Cs) and $K_{10}Tl_7$ [12–15]. The latter compound contains $[Tl_7]^{7-}$ pentagonal bipyramids as an exclusive thallium substructure and an excess of potassium atoms [15]. In 2024, the electron-precise, salt-like $Cs_{3.45}K_{3.55}Tl_7$ has been reported and represents only the second alkali metal thallide with $[Tl_7]^{7-}$ cluster as the exclusive cluster type [16].

If transition metals are added to the alkali metal triel mixtures, further compounds and sometimes even new cluster types can be obtained, which contain the transition metal as an endohedral atom like in $K_8Tr_{10}M$ (Tr=*Tl* M = Zn [17], Ga [18]; Tr = In, M = Zn [19]) or $A_{10}Tr_{10}M$ (A = K, Tr = In, M = Ni, Pd, Pt [20]; A = Na, Tr = Ga, M = Ni [21]). A_8Tr_{11} (A = K-Cs) is also known for indium in the case of potassium and rubidium [12, 22]. By substituting one indium by mercury in this system, the $[In_{11}]^{7-}$ cluster changes to $[In_{10}Hg]^{8-}$ with mixed-occupied positions and the compound becomes electron precise in terms of a salt-like description, according to the Zintl-Klemm-Busma concept [23].

Concerning thallides, an alternative option according to the already mentioned $K_8In_{10}Hg$ is represented by the examples $Na_9K_{16}Tl_{18}Cd_3$, or $K_{18}Tl_{20}Au_3$, [23–25] where the transition

In memory of Prof. Dr. H. Hillebrecht.

metal atoms together with thallium atoms form the cluster. Despite the options to have a transition element endohedral in a cluster or as part of a cluster, $K_{18}Tl_{20}Au_3$ represents an example of the third possibility, which occurs as a special feature for the element gold in alkali metal thallides. A special role can be expected for this element, as due to its highest electron affinity among the metals, it is capable of forming gold anions, so-called aurides [26]. In general, the formation of double salts has already been proven as a powerful tool to realize electron-precise Zintl phases for alkali metal tetrelides $[Tt_4]^{4-}$ [27–31]. Within the alkali metal thallium system, $[Tl_6]^{6-}$ clusters have been realized in double salt structures [32–34]. The combination with auride was already proven for $K_{18}Tl_{20}Au_3$ or $Na_{12}K_{38}Tl_{48}Au_2$ [24, 35], while only the latter one is reported as electron precise, including $[Tl_7]^{7-}$ and/or $[Tl_9]^{9-}$ clusters.

In this article, we present single-crystal X-ray structure analysis and DFT calculations of the electron-precise double salt $Cs_{3.4}K_{4.6}[Au][Tl_7]$, including $[Tl_7]^{7-}$ and $[Au]^-$ anionic moieties.

2 | Results and Discussion

2.1 | X-Ray Structure Analysis

The new quaternary compound $Cs_{3.4}K_{4.6}[Au][Tl_7]$ was first observed in a sample targeting the nominal composition $Cs_9K_9Tl_{20}Au_2$. Subsequently, stoichiometric samples have been prepared with the nominal compositions $Cs_7K_9Tl_{14}Au_2$ and $Cs_{6.87}K_{9.13}Tl_{14}Au_2$. The bulk material was characterized by powder diffraction analysis and always showed the presence of the side phases $K_{8-x}Cs_xTl_{11}$ and/or $K_{18-x}Cs_xTl_{20}Au_{3-y}$ (see Figure 1) [12, 13, 14, 24].

The compound $Cs_{3.4}K_{4.6}AuTl_7$ crystallizes in a new structure type in the orthorhombic space group *Pnma*. The crystallographic data are shown in Table 1, and the atomic coordinates and anisotropic displacement parameters are given in Supporting Information (Tables S1 and S2, Supporting Information).

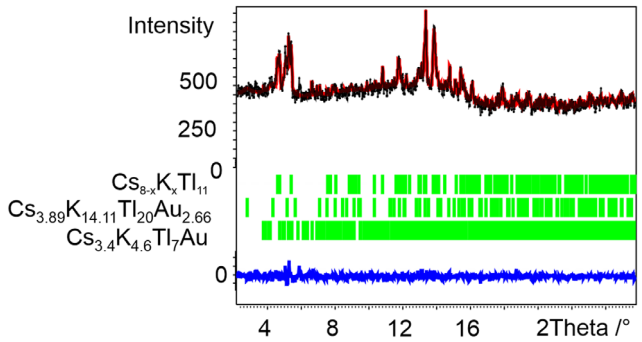

FIGURE 1 | Measured powder diffraction pattern of the approach with the nominal composition $Cs_9K_9Tl_{20}Au_2$ (black). The refinement was carried out with the LeBail algorithm in *Jana2006*. The calculated reflection positions are shown by the vertical bars (green) underneath the powder pattern. The curve at the bottom (blue) represents the difference plot. GOF = 0.73, $R_p = 2.25$, $R_{wp} = 3.44$.

TABLE 1 | Crystallographic data of $Cs_{3.4}K_{4.6}[Au][Tl_7]$.

Empirical Formula	**$Cs_{3.4}K_{4.6}AuTl_7$**
CSD Number	2 472 350
Formula Weight	4524.95
Temperature/K	123
Crystal System	orthorhombic
Space Group	*Pnma*
a/Å	39.6898(12)
b/Å	12.0407(4)
c/Å	10.9334(3)
Volume/Å^3	5225.0(3)
Z	8
P_{calc}/(g/cm^3)	5.752
μ/mm^{-1}	54.022
F(000)	7373.0
Crystal Size/mm^3	0.05 × 0.037 × 0.034
Radiation, λ/Å	Mo-Kα, 0.71073
2θ range for data/°	4.254–59.148
Index ranges	$-55 \le h \le 55$
	$-16 \le k \le 16$
	$-15 \le l \le 15$
Collected/Independent Reflections	50 338/7650
Data/Restraints/Parameters	7650/0/174
Goodness-of-fit on F^2	1.371
R_{int}	0.0544
R_1,wR_2 [I≥2σ(I)]	0.0477, 0.0915
R_1, wR_2 [all data]	0.0556, 0.0935
Largest diff. peak/hole/e Å^{-3}	3.49/−3.42

2.2 | Structure Description

2.2.1 | Anionic Substructures

The asymmetric unit of $Cs_{3.4}K_{4.6}[Au][Tl_7]$ contains twelve thallium atoms, eleven alkali metal atoms, and one gold atom, which reside on general as well as special Wyckoff positions of space group *Pnma*, and the unit cell content is completed by symmetry operations of the respective space group (see Figure 2). The thallium atoms form two crystallographically different pentagonal bipyramidal clusters, which consist of six symmetry-independent thallium positions each. According to a $Z = 4$, the empirical formula calculates to $Cs_{6.87}K_{9.13}Tl_{14}Au_2$, which can be reduced by

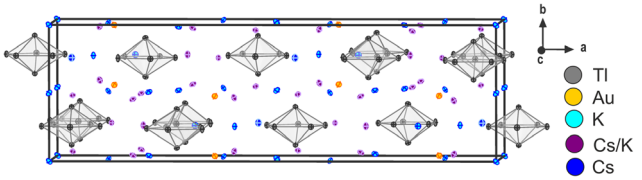

FIGURE 2 | Unit cell of $Cs_{3.4}K_{4.6}[Au][Tl_7]$.

two to the given composition. The shape of the clusters is according to those present in $K_{10}Tl_7$, $Na_9K_{16}Tl_{\sim 25.25}$, $Na_{12}K_{38}Tl_{48}Au_2$, $Cs_{7.29}K_{5.71}Tl_{13}$, and $Cs_{3.45}K_{3.55}Tl_7$ (see Table S4, Supporting Information).[15,16,35,36]

The $[Tl_7]^{7-}$ clusters are arranged in distorted hexagonal layers, resulting in an ABAB stacking sequence perpendicular to the crystallographic *b*-axis, which corresponds to a distorted hexagonal close packing. The gold atoms are located in the octahedral voids of the hcp arrangement of the pentagonal bipyramids, so that a NiAs structure is obtained, whereby the $[Tl_7]^{7-}$ clusters correspond to the arsenic atoms and the gold atoms to the nickel atoms (see Figure 3) [37].

The $[Tl_7]^{7-}$ clusters are surrounded by 24 and 21 alkali metal atoms, respectively (Figure 4). In both cases, the triangular faces between the equatorial and apical thallium atoms are μ_3-coordinated by one alkali metal each.

In the case of the pentagonal bipyramid 1, which consists of the thallium atoms Tl1 (Wyckoff 8*d*), Tl3, Tl4, Tl5, Tl6, and Tl11 (Wyckoff 4*c*), the equatorial edges Tl3-Tl11, Tl11-Tl4, and Tl4-Tl6 are each μ_2-coordinated by one alkali metal atom. In addition, the remaining eleven alkali metal atoms are coordinated terminally to the thallium atoms, with two alkali metals each at Tl11 and Tl4.

The equatorial edges Tl8-Tl10 and Tl9-Tl12 of the pentagonal bipyramid 2 are μ_2-capped, and eight alkali metal atoms coordinate to the thallium vertices, with none coordinating to Tl8 and three coordinating to Tl10.

In addition to the anionic thallium clusters, an $[Au]^-$ is also present. The gold position (Wyckoff 8*d*) is surrounded by four potassium atoms and two or four mixed-occupied alkali metal atoms in a distorted trigonal prism or square antiprism (see Figure 5). The distances are *d*(Au-K) = 3.270(3)−3.664(3) Å and *d*(Au-Cs/K) = 3.4424(8)−3.9613(14) Å. Two alkali metals of the coordination spheres of the gold atoms share the K8-K9 edge, so a dinuclear unit is formed, which again connects via Cs4/K6 to another dinuclear unit. Those chains lie along the crystallographic *b*-axis. This structural motif is not yet known from the literature.

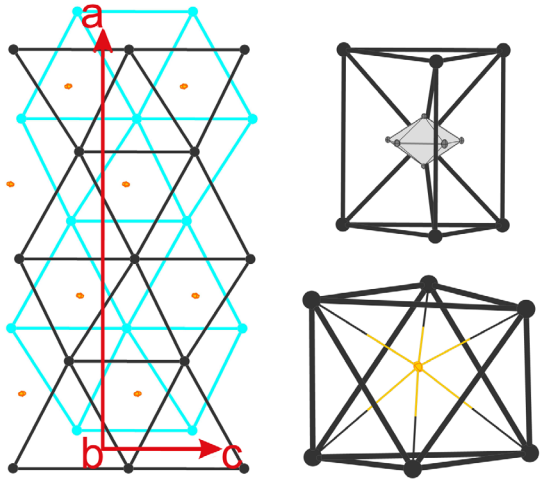

FIGURE 3 | Hexagonal layers of the $[Tl_7]^{7-}$ clusters in an ABAB stacking order (black and blue) and the gold atoms in the octahedral voids of the distorted hcp.

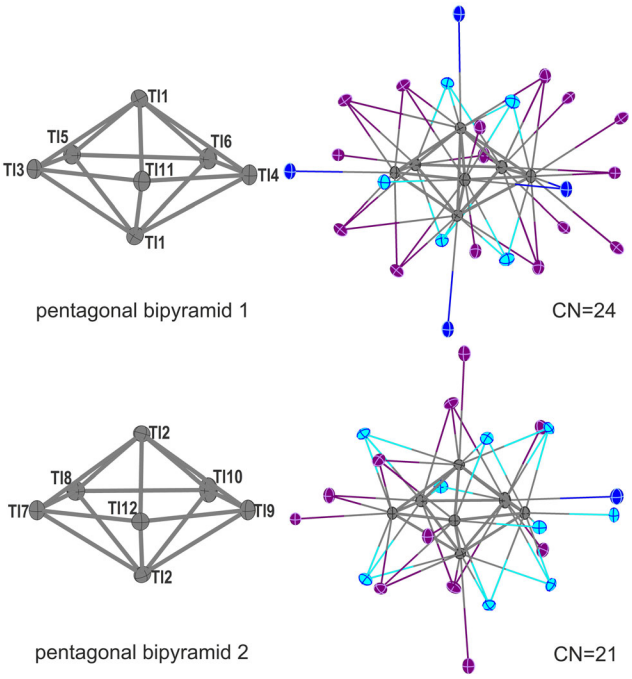

FIGURE 4 | The two crystallographically different $[Tl_7]^{7-}$ clusters together with their first coordination sphere.

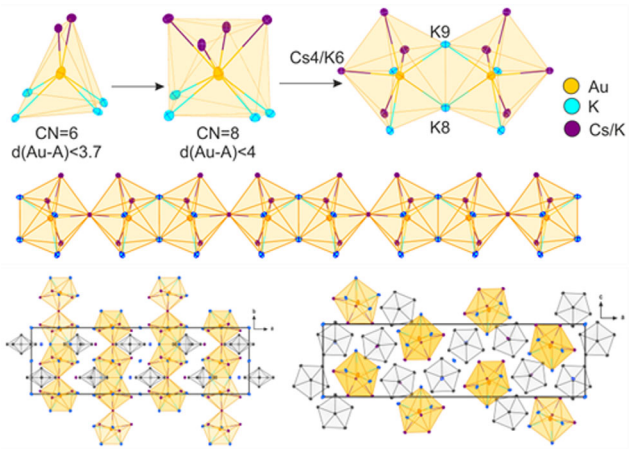

FIGURE 5 | First coordination sphere of the gold atom, which forms a dinuclear unit and with that even a chain. Additionally, the chains are depicted in the unit cell along the crystallographic *c*-axis (left) and *b*-axis (right).

Gold and thallium are indistinguishable by X-ray diffraction. For this reason, the distances to the alkali metals and the first coordination sphere need to be carefully examined. The surroundings of the gold atom (extended trigonal prism) show the typical arrangement known from literature, departing from alkali metal-gold-thallium compounds [24, 35]. The gold position shows a typical surrounding of aurides (CN = 6 or 8), which is not known for thallium. In the case of the cluster-forming thallium atoms Tl1-Tl12, a distorted icosahedral (CN = 12) or twice-capped square antiprismatic surrounding (CN = 10) is obtained (see Figure S1 in Supporting Information).

The similarity in the surroundings of the here-reported auride (see Figure 5) and the simplest alkali metal auride CsAu also supports the correct assignment in this case. For CsAu, a cubic coordination is present with distances d(Au-Cs) = 3.69 Å [38, 39]. In the related ammoniate CsAu·NH_3, the gold atom is surrounded trigonal prismatically by six cesium atoms (d(Au-Cs) = 3.59(2)−3.717(8) Å) and two additional gold atoms [40]. In case of the potassium aurides K_xAu_y, mainly layers or three-dimensional networks of gold and potassium in the voids are known, for example, in KAu_2 and K_2Au_3 [41, 42]. This increases the CN to a total of ten or twelve with distances of d(Au-K) = 3.301(2)−3.890(6) Å [41, 42].

In alkali metal thallides $Na_{12}K_{38}Tl_{48}Au_2$ [35], $K_{18}Tl_{20}Au_3$ [24], gold is surrounded by nine or ten atoms, which are arranged in a three or four-times-capped trigonal prism. Altogether, the trigonal prismatic surrounding of gold atoms is a common feature in these structures. In contrast, trigonal prismatic thallium coordination is uncommon and suspicious. This careful analysis allows the unquestionable assignment, despite the missing additional analytics due to extremely sensitive crystals and the lack of phase purity of the bulk material.

2.2.2 | Alkali Metal Coordination

The eleven crystallographically different alkali metal positions can be divided into five potassium positions, one cesium position, and five mixed-occupied positions of potassium and cesium. Furthermore, the alkali metals can be subdivided based on the coordination number of their first coordination sphere and the number of surrounding thallium clusters (see Figure 6).

The alkali metal positions K4, K5, and K8-K10 show coordination numbers between twelve and 15 and are each surrounded by two $[Tl_7]^{7-}$ clusters. The remaining alkali metal atoms complete the coordination sphere derived from an icosahedron. The next higher coordination numbers, 15 and 16, belong to the mixed-occupied positions. In the surrounding of Cs1/K1 (Wyckoff 8d), Cs2/K2 (Wyckoff 8d). Cs3/K3 (Wyckoff 8d), and Cs4/K6 (Wyckoff 4c), there are three thallium units each, and five clusters coordinate to position Cs5/K7 (Wyckoff 4c). The thallium clusters are arranged in a trigonal bipyramidal arrangement around Cs5/K7. A similar coordination sphere is also found at position Cs6 (Wyckoff 4c). Here, only the number of alkali metal atoms is increased by two, expanding the coordination sphere and allowing complete occupation by cesium. As in the previously reported compounds with mixed-occupied alkali metal positions, the trend continues [16, 43]: the higher the coordination number, the higher the proportion of the heavier alkali metal. The site occupancy factors of the individual alkali metal positions are listed in Table 2.

TABLE 2 | Site occupancy factors (s.o.f.) for the eleven crystallographically different alkali metal positions in $Cs_{3.4}K_{4.6}AuTl_7$.

s.o.f.	K	Cs	s.o.f.	K	Cs
Cs1/K1	0.095(7)	0.905(7)	Cs5/K7	0.044(10)	0.956(10)
Cs2/K2	0.454(7)	0.546(7)	Cs6	0	1
Cs3/K3	0.276(7)	0.724(7)	K8	1	0
K4	1	0	K9	1	0
K5	1	0	K10	1	0
Cs4/K6	0.416(9)	0.584(9)	–	–	–

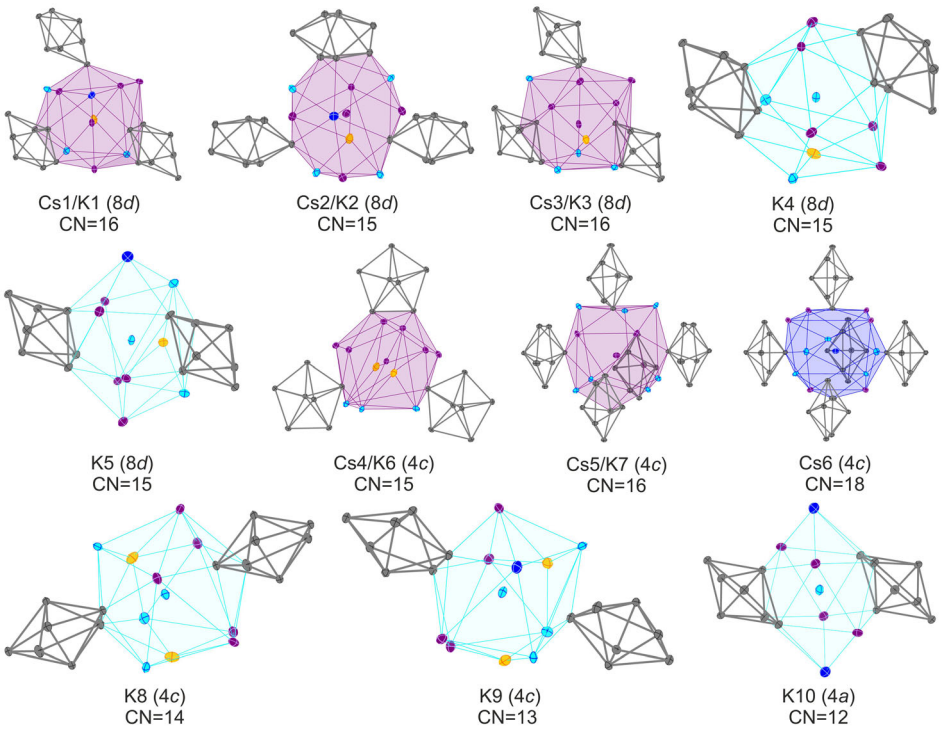

FIGURE 6 | First coordination sphere of the eleven crystallographically different alkali metal positions.

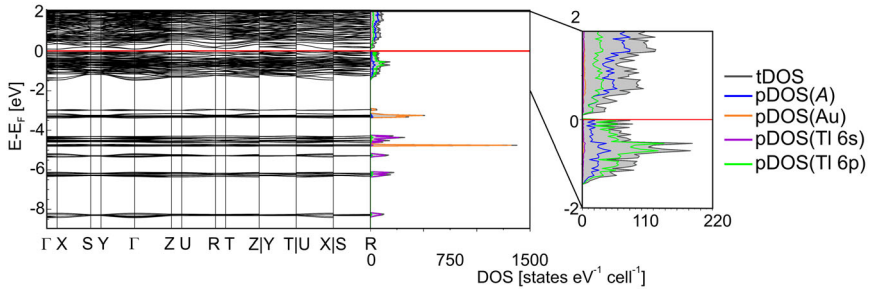

FIGURE 7 | Band structure and DOS of $Cs_{6.87}K_{9.13}Tl_{14}Au_2$.

2.3 | Calculations of the Electronic Structures

Band structure calculations were performed for the fully occupied approximant $Cs_7K_9Tl_{14}Au_2$, in which all mixed alkali metal positions are occupied by the main component Cs or K. The band structure shows a small bandgap of 0.10139 eV at the Fermi level. The states below E_F (<0 eV) are dominated by thallium 6p states. Between −9 and −3 eV, localized states can be found that can be assigned to gold (approx. −5 eV and between −4 and −3 eV) and mainly to the thallium 6s states (see Figure 7). The result affirms a description of the compound according to the Zintl-Klemm-Busmann concept, the molecular formula can be written as $[Cs^+]_{3.4}[K^+]_{4.6}[Au^-][Tl_7{}^{7-}]$.

3 | Conclusion

We here report on the synthesis and characterization of a thallide-auride double salt $[Cs^+]_{3.4}[K^+]_{4.6}[Tl_7{}^{7-}][Au^-]$. Single crystal X-ray structure analysis reveals the presence of $[Tl_7]^{7-}$ pentagonal bipyramidal clusters, which are known from $Na_9K_{16}Tl_{\sim 25.25}$, $Na_{12}K_{38}Tl_{48}Au_2$, $K_{10}Tl_7$, $Cs_{7.29}K_{5.71}Tl_{13}$, and $Cs_{3.45}K_{3.55}Tl_7$. Together with the latter compound, the new double salt is yet only the second electron-precise compound with $[Tl_7]^{7-}$ as an exclusive anionic cluster type. As a second anionic entity, an auride is present. Both anionic moieties are arranged in a distorted NiAs structure. Theoretical calculations reveal a small bandgap for the approximant $Cs_7K_9Tl_{14}Au_2$ at E_F and are in agreement with a salt-like description according to the Zintl–Klemm–Busmann concept.

4 | Experimental Section

4.1 | Materials

Potassium (purity: 99%, under mineral oil, Merck/Sigma–Aldrich, Darmstadt) was segregated for purification. Cesium was obtained by reduction of CsCl with elemental calcium and purified by distillation twice [44]. Thallium drops (purity 99.999%, ABCR) and gold wire (purity 99.999%, ABCR) were used without further purification and stored under an inert gas atmosphere.

4.2 | Preparation

For the nominal compositions of the approaches $K_9Cs_9Tl_{20}Au_2$ (m(Tl) = 0.692 g, m(K) = 0.060 g, m(Cs) = 0.202 g, m(Au) = 0.067 g), $K_9Cs_7Tl_{14}Au_2$ (m(Tl) = 0.680 g, m(K) = 0.084 g, m(Cs) = 0.221 g, m(Au) = 0.09437 g), and $K_{9.13}Cs_{6.87}Tl_{14}Au_2$ (m(Tl) = 0.677 g, m(K) = 0.084 g, m(Cs) = 0.216 g, m(Au) = 0.0932 g), the elements were placed in tantalum ampoules and sealed under an argon atmosphere. The sealed ampoules were placed in quartz glass tubes (QSIL GmbH, Ilmenau, Germany) and sealed under an argon atmosphere. The so-prepared ampoules were placed in an oven with the following temperature program: after heating to 773.15 K and holding for 2 days, the ampoule was cooled back to room temperature with 3 K per hour steps. The received products are very sensitive to moisture and oxygen. Therefore, they were stored in a glove box (Labmaster 130 G, Fa. M. Braun, Garching, Germany).

4.3 | X-Ray Single Crystal Analysis

A small number of crystals were transferred into dried mineral oil. A suitable crystal was selected and mounted on a *Rigaku XtaLAB* Synergy R DW diffractometer (Rigaku Polska sp. Z. o. o. UI, Wroclaw, Poland) (X-ray: rotating anode dual wavelength Cu and Mo, HyPix Arc 150° detector) using MiTeGen loops. All data were collected at 123 K.

CrysalisPro (Version 171.43.105a) was used for data collection and data reduction [45]. ShelXT was used for the structure solution, and the subsequent data refinement was carried out with *ShelXL* [46, 47]. *Olex*^{2} was taken for visualization purposes, and the software *Diamond4* was chosen for the representation of the crystal structure [48–50]. All atoms are depicted as ellipsoids with a 50% probability level.

Crystallographic data for the compound $Cs_{3.4}K_{4.6}Tl_7Au$ have been deposited in the Cambridge Crystallographic Data Center, CCDC, 12 Union Road, Cambridge CB21EZ, UK. Copies of the data can be obtained free of charge under the depository number CCDC-2 472 350 (Fay: +44-1223-336−033, E-Mail: deposit@ccdc.cam.ac.uk, http://www.ccdc.cam.ac.uk).

4.4 | Powder Diffraction Studies

Powder diffraction samples were prepared in sealed capillaries (Ø 0.3 mm, WJM-Glas-Müller GmbH, Berlin, Germany). The data collection was carried out on a STOE Stadi P diffractometer (STOE, Darmstadt, Germany)(Monochromatic MoKα1 radiation, $\lambda = 0.70926$ Å) equipped with a Dectris Mythen 1 K detector. For

visualization and indexation, the software *WinXPOW* and *Jana2006* were used [51, 52].

4.5 | Band Structure Calculations

Theoretical calculations were performed on the hypothetical compound $Cs_7K_9Tl_{14}Au_2$ with fully occupied alkali metal positions. The program *FPLO21* was used, which is based on the full-potential nonorthogonal local orbital minimum-basis within the generalized gradient approximation for the full-relativistic mode [53–56]. A full relativistic approach is necessary due to the high spin–orbit coupling of heavy elements (Cs, Au, Tl) in this compound. The exchange correlation was assumed in the form proposed by Perdew, Burke, and Ernzerhof (PBE) [57]. For the calculation of the density of states (DOS) and the band structure, a modular grid for the reciprocal space of $6 \times 6 \times 6$ k-points was used. For the visualization of the DOS, the program *Origin2022* (version 9.9.0.225), and for the band structure, the in *FPLO21* implemented program *xfbp* was used [58].

Acknowledgments

The authors thank Prof. Dr. N. Korber and Prof. Dr. A. Pfitzner for providing lab equipment. This research was funded by the Deutsche Forschungsgemeinschaft (DFG, German Research Foundation) – project 468336522) and the Hans-Böckler Foundation (Maria-Weber-Grant for S.G.).

Open Access funding enabled and organized by Projekt DEAL.

Funding

This work was supported by Deutsche Forschungsgemeinschaft (468336522).

Conflicts of Interest

The authors declare no conflicts of interest.

Data Availability Statement

The data that support the findings of this study are available in the supplementary material of this article.

References

1. R. Pöttgen and D. Johrendt, Intermetallics (deGruyter, Berlin/Boston, 2019).

2. E. Zintl, J. Goubeau, and W. Dullenkopf, "Salzartige Verbindungen und Intermetallische Phasen des Natriums in flüssigem Ammoniak," *Zeitschrift für Physikalische Chemie A* 154 (1931): 1–46.

3. E. Zintl and H. Kaiser, "Über die Fähigkeit der Elemente zur Bildung negativer Ionen," *Zeitschrift Fur Anorganische Und Allgemeine Chemie* 211 (1933): 113–131.

4. R. Nesper, "The Zintl-Klemm Concept-A Historical Survey," *Zeitschrift Fur Anorganische Und Allgemeine Chemie* 640 (2014): 2639–2648.

5. E. Zintl and W. Dullenkopf, "Über den Gitterbau von NaTl und seine Beziehung zu den Strukturen vom Typus des ß-Messings: 4. Mitteilung über Metalle und Legierungen," *Zeitschrift für Physikalische Chemie B* 16 (1932): 195–205.

6. E. Zintl, "Intermetallische Verbindungen," *Angewandte Chemie* 52 (1939): 1–6.

7. J. D. Corbett, "Polyanionic Clusters and Networks of the Early p-Element Metals in the Solid State: Beyond the Zintl Boundary," *Angewandte Chemie International Edition* 39 (2000): 670–690.

8. S. Gärtner, "Spotlight on Alkali Metals: The Structural Chemistry of Alkali Metal Thallides," *Crystals* 10 (2020): 1013.

9. R. Pöttgen and D. Johrendt, Thallides (deGruyter, Berlin/Boston, 2019), 117–122.

10. Z. C. Dong and J. D. Corbett, "$A_{15}Tl_{27}$ (A=Rb, Cs): A Structural Type Containing Both Isolated Clusters and Condensed Layers Based on the Tl_{11} Fragment. Syntheses, Structure, Properties, and Band Structure," *Inorganic Chemistry* 35 (1996): 1444–1450.

11. V. F. Schwinghammer, S. M. Tiefenthaler, and S. Gärtner, "The Role of Different Alkali Metals in the $A1_5Tl_{27}$ Type Structure and the Synthesis and X-ray Structure Analysis of a New Substitutional Variant $Cs_{14.53}Tl_{28.4}$," *Materials* 14 (2021): 7512.

12. W. Blase, G. Cordier, V. Müller, U. Häussermann, R. Nesper, and M. Somer, "Präparation und Kristallstrukturen von Rb_8In_{11}, K_8Tl_{11} und Rb8Tl_{11} sowie Bandstrukturrechnungen zu K8In_{11}," *Zeitschrift Fur Naturforschung, Teil B* 48 (1993): 754–760.

13. G. Cordier and V. Müller, "Crystal Structure of Octapotassium Undecathallide, K_8Tl_{11}," *Zeitschrift für Kristallographie* 198 (1992): 281–282.

14. Z.-C. Dong and J. D. Corbett, "A_8Tl_{11} (A=K, Rb, or Cs) Phases with Hypoelectronic Tl_{11}^{7-} Cluster Anions: Syntheses, Structure, Bonding, and Properties," *Journal of Cluster Science* 6 (1995): 187–201.

15. S. Kaskel and J. D. Corbett, "Synthesis and Structure of $K_{10}Tl_7$: The First Binary Trielide Containing Naked Pentagonal Bipyramidal Tl_7 Clusters," *Inorganic Chemistry* 39 (2000): 778–782.

16. V. F. Schwinghammer and S. Gärtner, "$[Tl_7]^{7-}$ Clusters in Mixed Alkali Metal Thallides $Cs_{7.29}K_{5.71}Tl_{13}$ and $Cs_{3.45}K_{3.55}Tl_7$," *Inorganic Chemistry* 63 (2024): 20078–20082.

17. Z. C. Dong, R. W. Henning, and J. D. Corbett, "$K_8Tl_{10}Zn$: A Zintl Phase Containing the Zinc-Centered Thallium Polyanion $Tl_{10}Zn_{(8-)}$," *Inorganic Chemistry* 36 (1997): 3559–3561.

18. B. Lehmann and C. Röhr, "Endohedral Ten-Vertex Clusters $[Ga@Tl_{10}]^{8-}$ in the Mixed Trielides A_8GaTl_{10} (A=K, Rb, Cs)," *Zeitschrift Fur Anorganische Und Allgemeine Chemie* 648 (2022): e202200204.

19. S. C. Sevov and J. D. Corbett, "Potassium Indium Zinc Compound $K_8In_{10}Zn$: Interstitially-Stabilized Analogs of Early-Transition-Metal Halide Clusters," *Inorganic Chemistry* 32 (1993): 1059–1061.

20. S. C. Sevov and J. D. Corbett, "$K_{10}In_{10}Z$ (Z= Ni, Pd, or Pt): Zintl Phases Containing Isolated Decaindium Clusters Centered by Transition Elements," *Journal of the American Chemical Society* 115 (1993): 9089–9094.

21. R. W. Henning and J. D. Corbett, "Formation of Isolated Nickel-Centered Gallium Clusters in $Na_{10}Ga_{10}Ni$ and a 2-D Network of Gallium Octahedra in K_2Ga_3," *Inorganic Chemistry* 39 (1999): 3883–3888.

22. S. C. Sevov and J. D. Corbett, "A Remarkable Hypoelectronic Indium Cluster in K_8In_{11}," *Inorganic Chemistry* 30 (1991): 4875–4877.

23. S. C. Sevov, J. E. Ostenson, and J. D. Corbett, "$K_8In_{10}Hg$: A Zintl Phase with Isolated $In_{10}Hg$ Clusters," *Journal of Alloys and Compounds* 202 (1993): 289–294.

24. Z. C. Dong and J. D. Corbett, "$K_{18}Tl_{20}Au_3$, A Novel Derivative of K_8Tl_{11} with the Unprecedented Polyanion $Tl_9Au_2^{9-}$, the Parent Tl_{11}^{7-} and an Isolated Au− Ion," *Inorganic Chemistry* 34 (1995): 5042–5048.

25. D. P. Huang and J. D. Corbett, "$Na_9K_{16}Tl_{18}Cd_3$: A Novel Phase Containing $Tl_8Cd_3^{10-}$ and Tl_5^{7-} Clusters," *Inorganic Chemistry* 38 (1999): 316–320.

26. V. Smetana, M. Rhodehouse, G. Meyer, and A.-V. Mudring, "Gold Polar Intermetallics: Structural Versatility Through Exclusive Bonding, Motifs," *Accounts of Chemical Research* 50 (2017): 2633–2641.

27. G. Frisch, C. Hoch, C. Röhr, P. Zönnchen, K. D. Becker, and D. Niemeier, "Alkaline Metal Stannide-Stannates: 'Double Salts' with Zintl Sn_4^{4-} and Stannate SnO_3^{4-} Anions," *Zeitschrift Fur Anorganische Und Allgemeine Chemie* 629 (2003): 1661–1672.

28. C. Hoch and C. Röhr, "Alkalimetall-Stannid-Silicate und Germanate: 'Doppelsalze' mit dem Zintl-Anion $[Sn_4]^{4-}$," *Zeitschrift Fur Anorganische Und Allgemeine Chemie* 628 (2002): 1541–1547.

29. S. Hoffmann, T. F. Fässler, C. Hoch, and C. Röhr, "Alkali Metal Tetrelide-Tetrelates: "Double Salts" With $[E_4]^{4-}$ Zintl Anions (E=Si, Ge) and the First Dimeric Cyclotrisilicate Ions $[Si_6O_{17}]^{10-}$," *Angewandte Chemie International Edition* 40 (2001): 4398–4400.

30. V. Hlukhyy and T. F. Fässler, "At the Border of Intermetallic Compounds and Transition-Metal Oxides: Crystal Intergrowth of the Zintl Phase Cs_4Ge_9 and Cs_2WO_4 or Cs_3VO_4 as well as Nine-Atom Cluster Relocation in the Solid State," *Angewandte Chemie International Edition* 51 (2012): 742–747.

31. V. Hlukhyy, T. F. Fässler, S. Ponou, S. Lidin, N. P. Ivleva, and R. Niessner, "Extreme Differences in Oxidation States: Synthesis and Structural Analysis of the Germanide Oxometallates $A_{10}[Ge_9]2[WO_4]$ As Well As $A_{10+x}[Ge_9]2[W_{1-x}Nb_xO_4]$ with A=K and Rb Containing $[Ge_9]^{4-}$ Polyanions," *Inorganic Chemistry* 51 (2012): 4058–4065.

32. A. Karpov and M. Jansen, "$A_{10}Tl_6O_2$ (A=K,Rb) Cluster Compounds Combining Structural Features of Thallium Cluster Anions and of Alkali Metal Sub-Oxides," *Chemical Communications* 16 (2006): 1706–1708.

33. V. Saltykov, J. Nuss, and M. Jansen, "$Cs_{10}Tl_6SiO_4$, $Cs_{10}Tl_6GeO_4$, and $Cs_{10}Tl_6SnO_3$ - First Oxotetrelate Thallides, Double Salts Containing "Hypoelectronic" $[Tl_6]^{6-}$ Clusters," *Zeitschrift Fur Anorganische Und Allgemeine Chemie* 637 (2011): 1163–1168.

34. V. Saltykov, J. Nuss, U. Wedig, and M. Jansen, "Regular $[Tl_6]^{6-}$ Clusters in Cs_4Tl_2O Exhibiting Closed-Shell Configuration and Energetic Stabilization due to Relativistic Spin-Orbit Coupling," *Zeitschrift Fur Anorganische Und Allgemeine Chemie* 637 (2011): 357–361.

35. D. P. Huang, Z. C. Dong, and J. D. Corbett, "$Na_{12}K_{38}Tl_{48}Au_2$: A Metallic Zintl Phase with Naked Icosahedral Fragments Tl_7^{7-} and Tl_9^{9-} Plus Au^-," *Inorganic Chemistry* 37 (1998): 5881–5886.

36. B. Li and J. D. Corbett, "$Na_9K_{16}Tl_{\sim 25}$: A New Phase Containing Naked Icosahedral Cluster Fragments Tl_9^{9-}," *Journal of Cluster Science* 19 (2008): 331–340.

37. G. Aminoff, "XI. Untersuchungen über die Kristallstrukturen von Wurtzit und Rotnickelkies," *Zeitschrift für Kristallographie - Crystalline Materials* 58 (1923): 203–219.

38. U. Zachwieja, "Einkristallzüchtung und Strukturverfeinerung von RbAu und CsAu," *Zeitschrift Fur Anorganische Und Allgemeine Chemie* 619 (1993): 1095–1097.

39. A. Sommer, "Alloys of Gold with Alkali Metals," *Nature* 152 (1943): 215.

40. A. V. Mudring, M. Jansen, J. Daniels, et al., "Cesiumauride Ammonia (1/1), $CsAu*NH_3$: A Crystalline Analogue to Alkali Metals Dissolved in Ammonia?," *Angewandte Chemie International Edition* 41 (2002): 120–124.

41. K. J. Range, F. Rau, and U. Klement, "Potassium Digold, KAu_2," *Acta Crystallographica, Section C* 44 (1988): 1485–1486.

42. P. Krieger-Beck, A. Brodbeck, and J. Strähle, "Synthese und Struktur von K_2Au_3, einer neuen Phase im System Kalium-Gold," *Zeitschrift Fur Naturforschung, Teil B* 44 (1989): 237–239.

43. V. F. Schwinghammer, S. A. Khan, S. M. Tiefenthaler, T. Kovářík, J. Minár, and S. Gärtner, "Approaching Hypothetical RbTl in Experiments and Theory – X-ray Structure Determination of $Cs_{1-x}Rb_xTl$ (x = 0.18, 0.42) and a Solid Solution $K_{1-x}Rb_xTl(x \leq 0.69)$," *Inorganic Chemistry* 64 (2025): 6879–6887.

44. L. Hackspill, "Sur une nouvelle préparation du rubidium et du caesium," *Comptes Rendus Hebdomadaires des séances de l'Académie des Sciences* 141 (1905): 106.

45. M. W. Schneider, I. M. Oppel, A. Griffin, M. Masalerz, CrysalisPro, Version 171.43.105a (Oxford Diffraction/Agilent Technologies UK Ltd., Yarnton, UK, 2020).

46. G. M. Sheldrick, "Crystal Structure Refinement with SHELXL," *Acta Crystallographica, Section C* 71 (2015): 3–8.

47. G. M. Sheldrick, "SHELXT - Integrated Space-Group and Crystal-Structure Determination," *Acta Crystallographica, Section A* 71 (2015): 3–8.

48. L. J. Bourhis, O. V. Dolomanov, R. J. Gildea, J. A. K. Howard, and H. Puschmann, "The Anatomy of a Comprehensive Constrained, Restrained Refinement Program for the Modern, Computing Environment-Olex2 Dissected," *Acta Crystallographica, Section A* 71 (2015): 59–75.

49. O. V. Dolomanov, L. J. Bourhis, R. J. Gildea, J. A. K. Howard, and H. Puschmann, "OLEX2: A Complete Structure Solution, Refinement and Analysis Program," *Journal of Applied Crystallography* 42 (2009): 339–341.

50. K. Brandenburg, Diamond, Version 4.6.6 (Crystal Impact GbR, Bonn 2021).

51. A. Toombs, WinXPow, Version 3.4.6 (STOE & Cie GmbH, Darmstadt, 2016).

52. V. Petrícek, M. Dusek, and L. Palatinus, "Crystallographic Computing System JANA2006: General Features," *Zeitschrift für Kristallographie – Crystalline Materials.* 229 (2014): 345–352.

53. K. Lejaeghere, G. Bihlmayer, T. Bjorkman, et al., "Reproducibility in Density Functional Theory Calculations of Solids," *Science* 351 (2016): 7.

54. H. Eschrig, K. Koepernik, and I. Chaplygin, "Density Functional Application to Strongly Correlated Electron Systems," *Journal of Solid State Chemistry* 176 (2003): 482–495.

55. I. Opahle, K. Koepernik, and H. Eschrig, "Full-Potential Band-Structure Calculation of Iron Pyrite," *Physical Review B* 60 (1999): 14035–14041.

56. K. Koepernik and H. Eschrig, "Full-Potential Nonorthogonal Local-Orbital Minimum-Basis Band-Structure Scheme," *Physical Review B* 59 (1999): 1743–1757.

57. J. P. Perdew, K. Burke, and M. Ernzerhof, "Generalized Gradient Approximation Made Simple," *Physical Review Letters* 77 (1996): 3865–3868.

58. Origin2022, Version 9.9.0.225 (OriginLab Corporation, Northampton, MA, USA, 2022).

Supporting Information

Additional supporting information can be found online in the Supporting Information section. **Supporting Fig. S1:** First coordination spheres of the twelve crystallographically different thallium positions. **Supporting Table S1:** Fractional atomic coordinates and equivalent isotropic displacement parameters are defined as 1/3 of the trace of the orthogonalized U_{IJ} tensor. **Supporting Table S2:** Anisotropic displacement parameters. **Supporting Table S3:** Selected atomic distances in $Cs_{3.4}K_{4.6}Tl_7Au$. **Supporting Table S4:** Distances and distortion degree of already known $[Tl_7]^{7-}$ pentagonal bipyramids.